4

Fluorine based Organic Electrolyte for Ultrafast EDLCs

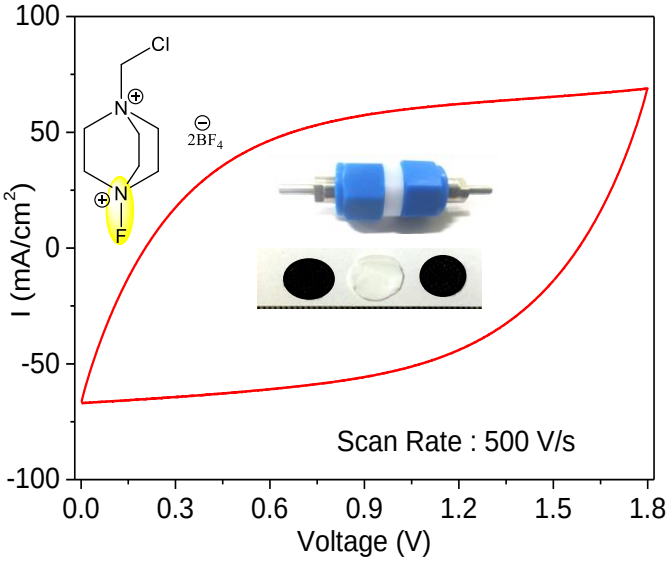

4.1 Introduction

Electric double layer capacitors (EDLCs) as an energy storage device have gained a lot of consideration [González et al., 2016; Iro et al., 2016; Lim et al., 2016; Wang et al., 2017a]. Very high power density and exceptional cyclability have led to their application in day-to-day devices such as flash light LEDs, electric and hybrid vehicles, uninterruptible power sources *etc.* [González et al., 2016; Kötz et al., 2000; Miller et al., 2008b, 2008a]. EDLCs stores energy by simple electrostatic adsorption and desorption of the electrolyte ion. Electrolyte in EDLC is one of the most significant component that have a direct influence on the characteristics of a supercapacitor [Béguin et al., 2014; Zhong et al., 2015]. The type and properties of the electrolytes directly influence the capacitance, resistance, stability, energy density, and power density of the EDLCs (Figure 4.1).

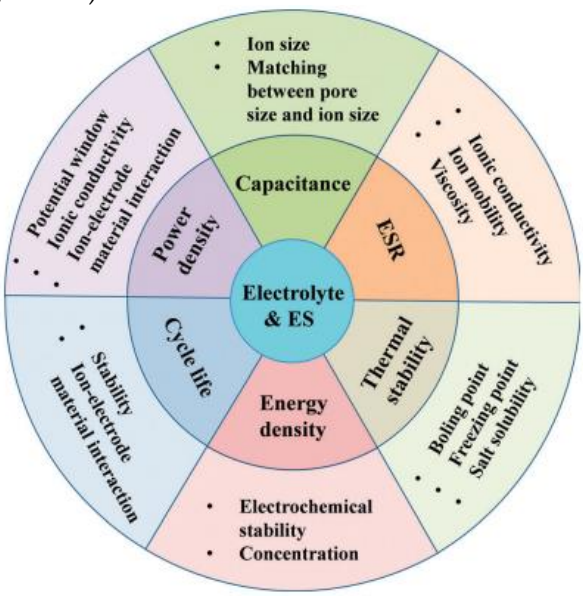

Figure 4.1: Role and effect of electrolytes on supercapacitor performance. Figure adapted from reference [Zhong et al., 2015].

Aqueous electrolytes are easy to handle, possess higher conductivity but suffer from limited voltage window of ~1.0 V [Zhao et al., 2015]. Organic electrolytes offer a wider voltage window of ~3-3.5 V at the cost of conductivity [Kurzweil et al., 2008]. Ionic liquids with lower melting point, lower volatility and higher temperature stability are quite attractive as electrolytes due to wider voltage window of ~4 V despite it being expensive with moderate conductivity [Gastol et al., 2016]. Despite of all the research efforts, EDLCs still suffer from limited capacitance, higher charging time and poor cyclability that limit its application in many areas. Depending on various applications, electrode materials and devices, each electrolyte exhibit their own advantages and disadvantages. For this reason there has been a constant urge to develop and explore new electrolyte systems for improving the overall supercapacitive performance of electrical double layer supercapacitors.

Fluorine-based cationic electrolyte in an EDLC supercapacitor can be a new approach for optimizing their efficiency. Fluorine, being the most electronegative in the periodic table provide a dense-packing to the molecule itself and thus enhancing the mobility of the electrolyte in the presence of external field. Moreover, fluorine containing organic compounds are thermally and electrochemically stable and thus can be exploited over wider ranges of temperature and voltage [Ohmi et al., 2013]. In the literature, fluorine containing electrolyte such as fluorinated carbonates and ethers, doped barium fluoride salts ($Ba_{1-x}La_xF_{2+x}$) has been proved to have higher energy density and longer retentivity in lithium ion batteries [Azimi et al., 2013; Rongeat et al., 2013; Zhang et al., 2011, 2013]. Fluorinated molecules are considered as best candidate for high voltage electrolyte since these possess higher oxidation potentials due to the strong electron-withdrawing effect of the fluorine atom [Zhang et al., 2013]. Herein, we have reported application of electrophilic fluorine precursor, Selectfluor™ (F-TEDA) as an electrolyte component in supercapacitors. F-TEDA is a well-known source of electrophilic fluorine in organic reactions [Naveen et al., 2017; Xing et al., 2015]. F-TEDA does not require any special handling conditions and is highly stable *bench-top* reagent unlike the conventional toxic and explosive sources of fluorine.

4.1.1 Objectives of Work:

The objectives of this work are as follows:

1. To explore novel fluorine based electrolytic system with F-TEDA (Selectfluor™) as a mixture electrolyte in tetrabutyl ammonium tetrafluoroborate ($TBABF_4$) salt as an electrolyte.

2. To study the capability of mixture electrolyte for enhanced specific capacitance, high rate capability, and stability in EDLC device.

3. To characterize EDLC devices in ambient and inert conditions to analyzing the effect of moisture content on EDLC performance.

4.2 Experimental

4.2.1 Material

F-TEDA/$TBABF_4$ electrolyte mixture was prepared by dissolving 0.06 mmol of F-TEDA (21.9 mg, Sigma Aldrich, CAS No. 140681-55-6) and 0.44 mmol $TBABF_4$ (144.24 mg, Sigma Aldrich, CAS No. 429-42-5) in 1 mL of anhydrous acetonitrile (99.8%) to form 0.5 M solution. The F-TEDA solution of higher concentration could not be obtained due to its own solubility limit and common ion effect of BF_4^- in $TBABF_4$. Electrolyte solution of tetrabutylammonium tetrafluoroborate (0.5 M) was also prepared as control. Carbon cloth (CC) was purchased from Fuel Cell Earth LLC and used after cleaning with acetone and IPA solvent without any surface modification.

4.2.2 Ionic Conductivity Measurement

Ionic conductivity values of F-TEDA/$TBABF_4$ mixture and control $TBABF_4$ in acetonitrile were measured directly in solution using Oakton Conductivity Meter at 303 K and aliquot of deionized (DI) water was added to the electrolyte to study the relative effect of water content on conductivity values. The ionic conductivity of corresponding electrolyte was also measured at different temperatures (303 -353 K) by heating the electrolyte solution on hotplate.

4.2.3 Device Fabrication

Commercially available Celgard™ membrane of thickness 25 µm was used as a separator. A symmetric two electrode supercapacitor assembly was fabricated in Swagelok Cell using 8 mm diameter CC electrode and 10 mm diameter separator. The electrolyte (50 µL) was filled in between the electrodes inside the Swagelok-fitting to complete the device assembly. The device was assembled in ambient in order to study the effect of water that is usually present as moisture with RH of 45%. Similar devices were fabricated inside the argon filled glove box (H_2O < 0.1 ppm and O_2 < 0.1 ppm) to rule out the effect of water even in low quantities. Similar devices fabricated in Swagelok assembly were chosen as it gave an advantage of long term stability and tight contacts.

4.2.4 Electrochemical Measurements

Two electrode measurements were done on CH-660 electrochemical workstation. Cyclic Voltammetry profile was acquired in the potential range between 0-0.8 V and 0-1.8 V at different scan rates from 0.02-1000 V/s for ambient and inert conditions, respectively. Galvanostatic charge discharge (GCD) measurements were carried out at areal current densities from 0.1-10 mA/cm^2. Specific capacitances for all the cells were calculated using formula $C=2(J\Delta t/\Delta V)$ where J is discharge current density, Δt is the discharge time and ΔV is the corresponding voltage drop upon discharge. Electrochemical impedance analysis of the devices was performed in 0.1-10^6 Hz frequency range. The obtained data was fitted and analyzed using EIS spectrum analyser software for EIS parameters. All the measurements were performed over 5 different devices of same type and the data from best performing devices assembled under identical conditions are reported in this study.

4.3 Results and Discussion

4.3.1 Electrolyte Characterization

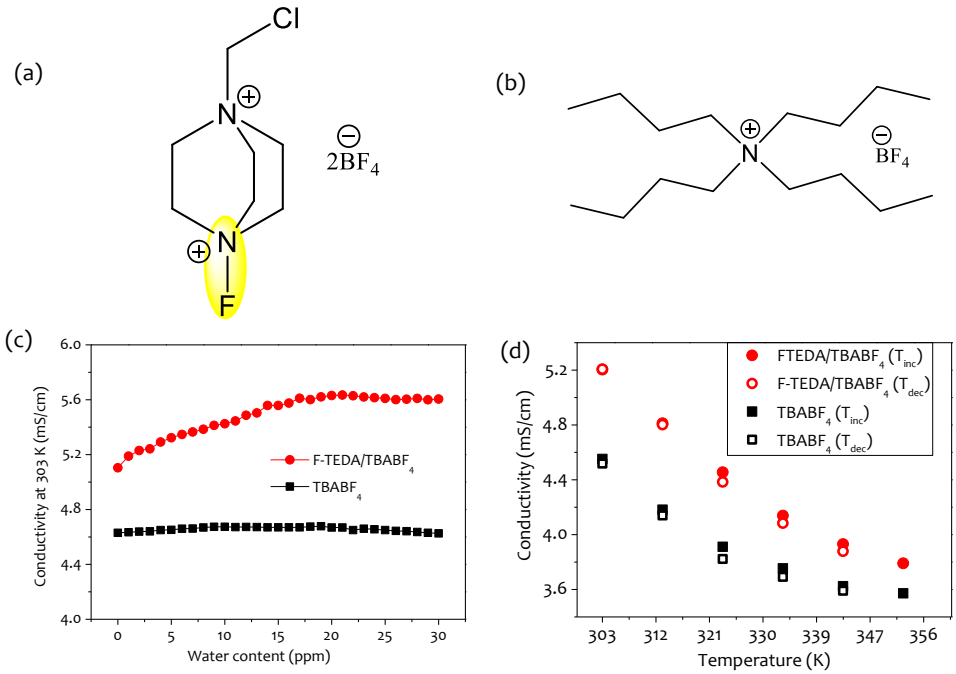

Figure 4.2: Chemical structure of (a) F-TEDA with polar N-F bond and (b) $TBABF_4$. Ionic conductivity of F-TEDA/$TBABF_4$ mixture and $TBABF_4$ in absence and presence of varying water content at 303 K. (d) Change in conductivity with increasing temperature of 0.5M F-TEDA/$TBABF_4$ mixture and $TBABF_4$.

The chemical structures of F-TEDA and $TBABF_4$ are shown in Figure 4.2 a,b respectively. F-TEDA was added as an additive electrolyte in conventional electrolyte, $TBABF_4$ and dissolved in acetonitrile to form the mixture electrolyte solution. The conductivity of 0.5 M F-TEDA/$TBABF_4$ electrolyte mixtures under inert conditions is 5.10 mS/cm which is higher than that of $TBABF_4$ (4.63 mS/cm). Overall, conductivity values are moderate and comparable to the value of organic electrolyte system used in literature [Zhong et al., 2015]. The conductivity of F-TEDA/$TBABF_4$ electrolyte mixture and $TBABF_4$ were measured for controlled aliquot of DI water added to the electrolyte solution (Figure 4.2c). With increasing volume of DI water in electrolyte mixture, the conductivity increases linearly from 5.10 mS/cm to a maximum value of 5.63 mS/cm. The increase in conductivity could be related to the water surrounding the F-TEDA molecules weakening the electrostatic interactions between the cations and anions in the electrolyte (Figure 4.2c). On contrary, there is no significant change in the conductivity of $TBABF_4$ which indicates specific interaction of water molecules with F-TEDA even in the presence of acetonitrile (Figure 4.2c). When the water content is beyond 16 ppm, the overall preferential water binding sites present in F-TEDA are saturated by water molecules and any further increase in water molecules does not affect the conductivity of the solution.
In the temperature dependent conductivity measurement, ionic conductivity decreases at higher temperature which is unlikely in solution based systems. It could be probably due to ion aggregation resulting in a decrease in mobility of ions [Abbott et al., 2000]. However, the temperature dependent change in conductivity observed in this case is reversible indicating no major cross-interaction occurs between F-TEDA/$TBABF_4$ mixture (Figure 4.2d).

4.3.2 Supercapacitor Geometry

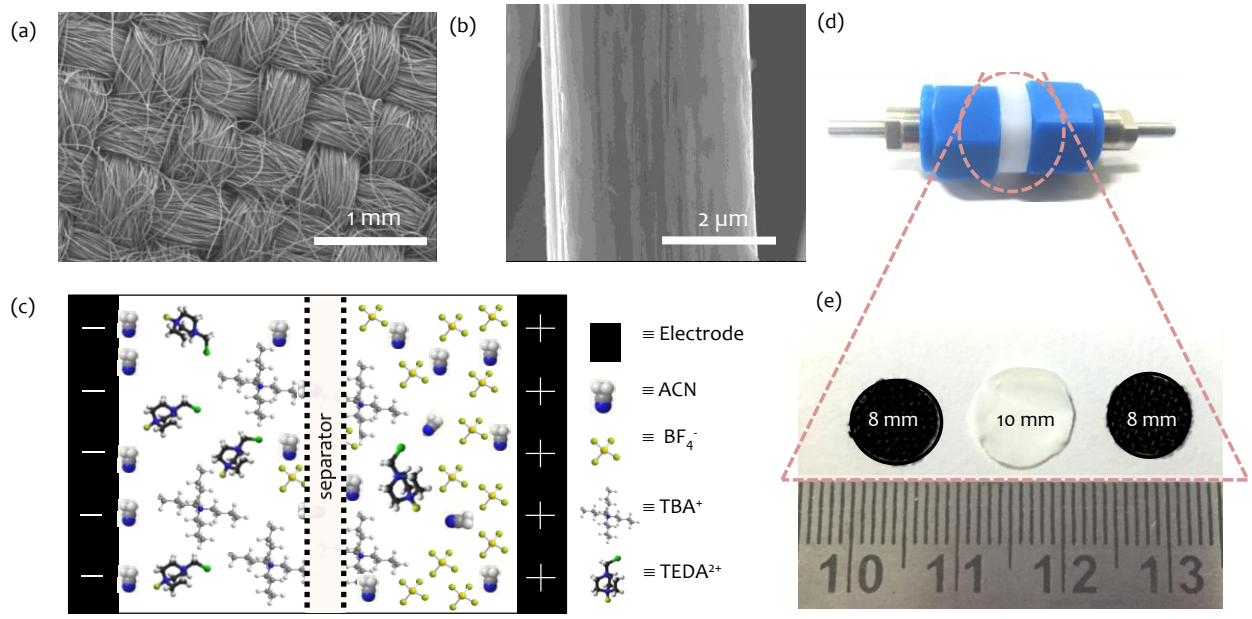

Figure 4.3: FESEM images of carbon cloth at (a) low and (b) high magnification. (c) Schematic of different components of supercapacitor. Photograph of (d) Swagelok-type supercapacitor assembly and (e) Carbon cloth electrodes and separator used in the study.

The two electrode supercapacitor assembly was made using conducting carbon cloth as an electrode material and F-TEDA/$TBABF_4$ mixture as electrolyte. The carbon cloth consists of interwoven carbon fibres of diameter ~4 µm (Figure 4.3a,b). Tetrabutylammonium tetrafluoroborate ($TBABF_4$) in acetonitrile (0.5 M) was used as a control electrolyte for comparison. Since the low water content affects the conductivity of electrolyte, devices were assembled inside and outside the glove box to analyse the effect of moisture under real conditions. Devices based on F-TEDA/$TBABF_4$ mixture and $TBABF_4$ assembled in ambient conditions were denoted as A:mixture (ambient) and B:control (ambient) while those assembled inside glove box were labelled as C:mixture (inert) and D: control (inert) respectively (Figure

4.3c). The Swagelok device, carbon cloth electrodes and Celgard seperator are shown in Figure 4.3d and e respectively.

4.3.3 Electrochemical Properties

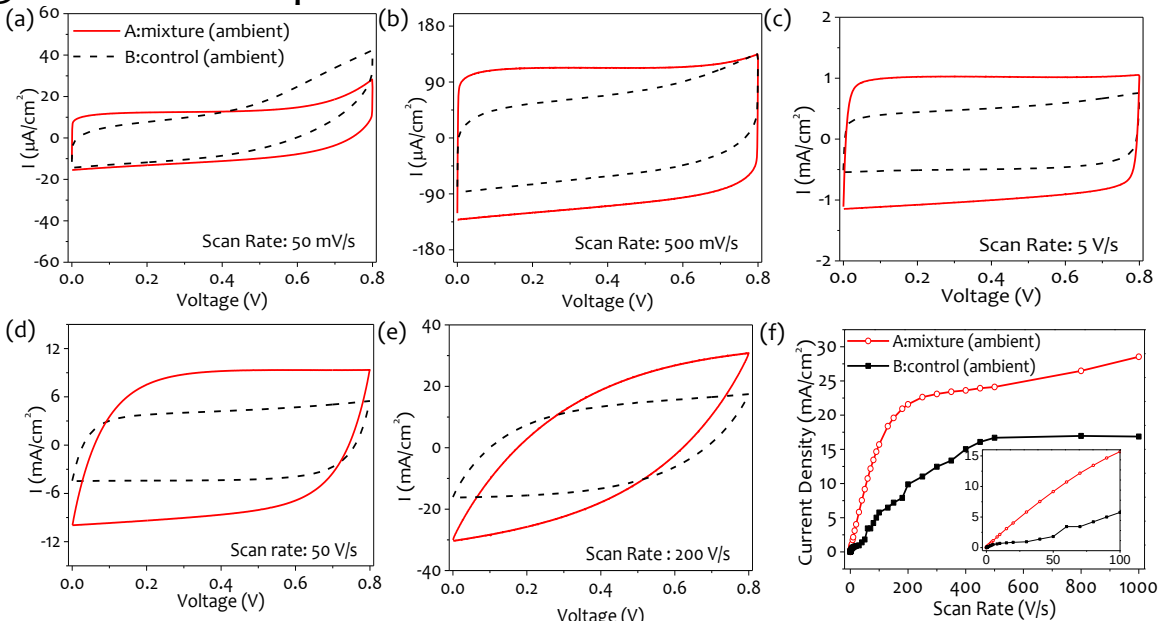

Figure 4.4: (a-e) Comparative cyclic voltammetry curves of supercapacitors assembled in ambient condition at scan rates of 50 mV/s, 500 mV/s, 5 V/s, 50 V/s and 200 V/s respectively. (f) Current density at 0.4 V for varying scan rates of 0.02-1000 V/s. Inset shows the magnified graph for the same. (Note: The legends are same for (a-e) as in (a)).

Cyclic Voltammetry (CV) of the two-electrode devices assembled in ambient was carried out at different scan rates to examine their capacitive behaviour (Figure 4.4). The voltage window was limited to 0.8 V in order to avoid electrolysis of water adsorbed on electrode as well as electrolyte under ambient conditions as the device behaves as an open system. The CV curves are rectangular in shape in wide range of scan rate (Figure 4.4a-d) revealing the electric double layer capacitive (EDLC) behaviour of mixed electrolyte and absence of redox activity of organo-fluorine compound in $TBABF_4$ (Figure 4.4 a-e). The device A with mixture electrolyte exhibits higher current density with respect to device B which is retained at all scan rates. This could be due to the reduction in the electrostatic interaction between ions as water molecules may possibly form a ligand shell around the F-TEDA cation resulting in an increase in mobility of ions thus increasing the overall current density. Similar effect of water on imidazolium based RTILs is predicted by MD simulations in literature [Hanke et al., 2003; Jiang et al., 2007]. Moreover, the rectangularity of the CV curve improves up to 5 V/s (Figure 4.4a-c) and beyond which it starts to deviate gradually (Figure 4.4d,e). The increase in current density is linear up to high scan rate of 200 V/s and 500 V/s for devices A and B respectively suggesting excellent charge propagation at electrode and electrolyte interface in both the devices (Figure 4.4f).

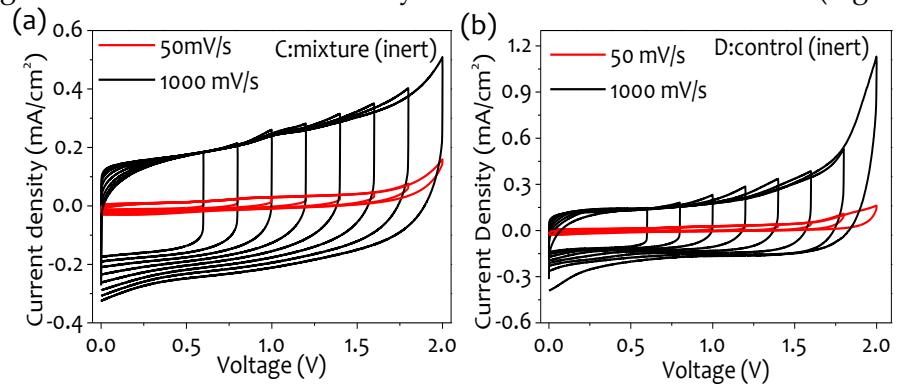

Figure 4.5: Cyclic Voltammetry curves of (a) C:mixture (inert) and (b) D:control (inert) at increasing voltage window.

To understand the behaviour of the devices in inert atmosphere, CV of the two-electrode devices assembled inside glove box were carried out. Though the voltage window in non-aqueous solvents is usually extended up to 2.7 V, in this case, it is restricted to 1.8 V to avoid the contribution of even the trace amount of water (Figure 4.5a,b). The gain in potential window (ΔE=1.0 V) is due to the absence of water content in inert atmosphere.

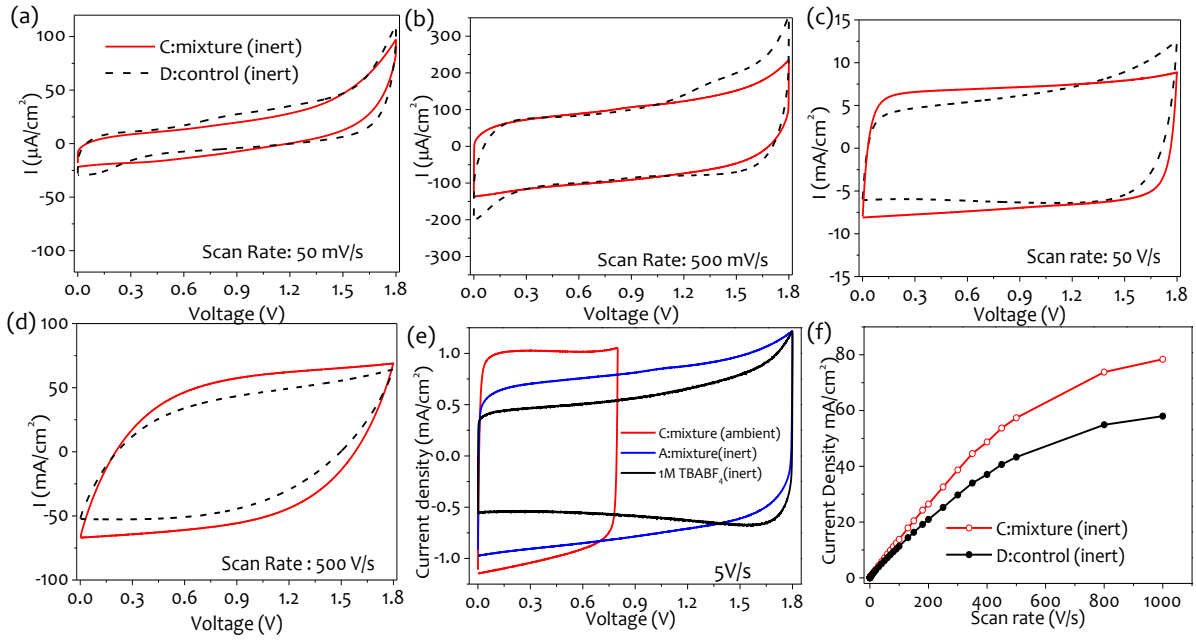

Figure 4.6: (a-d) Cyclic voltammetry curves of supercapacitors assembled inside glove box at scan rates of 50 mV/s, 500 mV/s, 50 V/s and 500 V/s respectively. (e) The electrochemical performance of device A and C compared with standard electrolyte (1M $TBABF_4$ in acetonitrile). (f) Current density at 0.9 V for varying scan rates of 0.02-1000 V/s. Note that the legends in (a-e) are same as in (a).

It is interesting to note that the relative difference in the current densities for devices C and D assembled in argon atmosphere is insignificant in comparison to the devices assembled in ambient (A and B) indicating towards the sensitivity of F-TEDA towards water (Figure 4.6a-d). Clearly, water interaction with F-TEDA is responsible for the increase in current density as observed in Figure 4.2c. The comparison of the electrochemical performance of device A and C is compared with increased concentration of standard electrolyte (1M $TBABF_4$ in acetonitrile) in Figure 4.6e. Further, in absence of water content, current density remains almost linear with respect to scan rate upto 500 V/s and deviates a little at higher scan rate of 1000 V/s, which is remarkable and noteworthy (Figure 4.6f). Such ultrahigh scan rate of 500 V/s is highest reported in literature for non-planar two-electrode volumetric supercapacitors (Table 4.1). Organic electrolytes with wider voltage window have large ions. The large ions with lower mobility cannot explores the narrow pores of electrodes at high scan rates. Aqueous electrolytes with small ions have increased mobility with high scan rates at the cost of limited voltage window.

Table 4.1: Literature survey of carbon material based supercapacitors.

No.	Electrode	Electrolyte	(ΔV)	υ (V/s)	Reference
1	Carbon fibre aerogel	6 M KOH	1	1	[Cheng et al., 2016a]
2	Reduced graphene oxide	25% KOH	0.8	400	[Sheng et al., 2012]
3	PEDOT coated MWNT	1M H_2SO_4	0.8	80	[Lee et al., 2013]
4	PEDOT coated MWNT	PVA-H_2SO_4	0.8	20	[Lee et al., 2013]
5	Carbon shell	6M KOH	1	0.5	[Yang et al., 2017]
6	Carbon shell	1 M $TEABF_4$	2.5	1	[Yang et al., 2017]

7	P and N-doped carbon nanosheets	6 M NaOH	1	2	[Jin et al., 2017]
8	Graphene coated carbonized cellulose	6M KOH	0.9	500	[Ren et al., 2016]
9	Activated graphene oxide	Gel polymer electrolyte	1.6	50	[Suleman et al., 2017]
10	Human hair/Ni/Graphene/MnO_2	PVA/KOH	1.8	20	[Liu et al., 2017b]
11	SWNT on Au coated stainless steel	0.5 H_2SO_4	1.0	1000	[Rangom et al., 2015]
12	CNT	1 M $TEABF_4$	2.5	450	[Yoo et al., 2015]
13	Ag NWs/3D-graphene foam/OMC	6M KOH	1	0.1	[Zhi et al., 2014]
14	Sawdust based microporous carbon	EMImTFSI	3	0.2	[Fuertes et al., 2015]
15	Sawdust based microporous carbon	EMImTFSI in acetonitrile	3	1	[Fuertes et al., 2015]
16	Sawdust based micro-mesoporous carbon	EMImTFSI	3	0.5	[Fuertes et al., 2015]
17	Sawdust based micro-mesoporous carbon	EMImTFSI in acetonitrile	3	2	[Fuertes et al., 2015]
18	N doped carbon fibres	2 M H_2SO_4	1	0.1	[Chen et al., 2017]
19	Activated graphene	$BMIMBF_4$ in acetonitrile	3.5	0.5	[Zhu et al., 2011]
20	Hierarchical Porous Graphitic Carbon	6M KOH	1	0.2	[Wang et al., 2008]
21	Graphene	30 wt % KOH	1	0.1	[Wang et al., 2009]
22	Carbon cloth	F-TEDA in $TBABF_4$	1.8	1000	This work

4.3.4 Energy Storage Performance

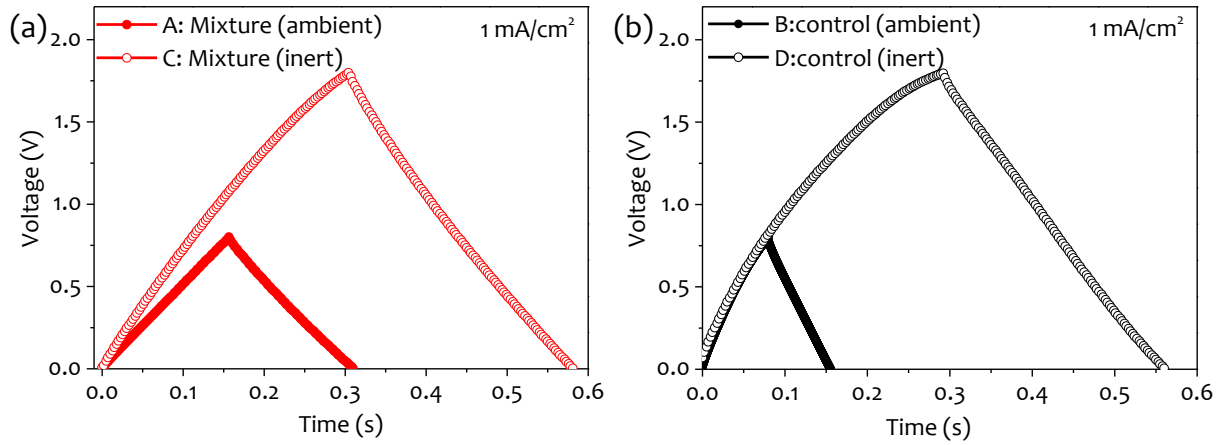

Figure 4.7: Galvanostatic charge/discharge (GCD) curves at current density of 1 mA/cm^2 of (a) device A:mixture (ambient) and C:mixture (inert), (b) device B:control (ambient) and D:control (inert).

To examine the energy storage capability, cyclic life stability and reversibility of the fabricated supercapacitors, galvanostatic charge/discharge (GCD) measurements were performed at

different current densities ranging between 0.1-10 mA/cm^2. At 10 mA/cm^2 and beyond, the charging occurs in few milliseconds and peak voltage decreases. As water content influences the performance of supercapacitor device with mixed electrolyte system, it is worthwhile to compare devices A and C assembled with mixed electrolyte in ambient and inert respectively. A comparison is also drawn for devices B and D based on $TBABF_4$ electrolyte in wet and dry state respectively. For both the devices A and C, charge discharge curves are triangular at current density of 1 mA/cm^2 however the voltage range of device C (1.8 V) is higher than device A (0.8 V) with negligible IR drop (Figure 4.7a). Interestingly, device C prepared in inert, exhibits higher charging rate despite of the same electrode and electrolyte configuration thus indicating faster ion transport. However, for devices B and D prepared in inert conditions, charging rate is exactly same (Figure 4.7b). It is also consistent with the insignificant change in conductivity values observed for $TBABF_4$ electrolyte in Figure 4.2c.

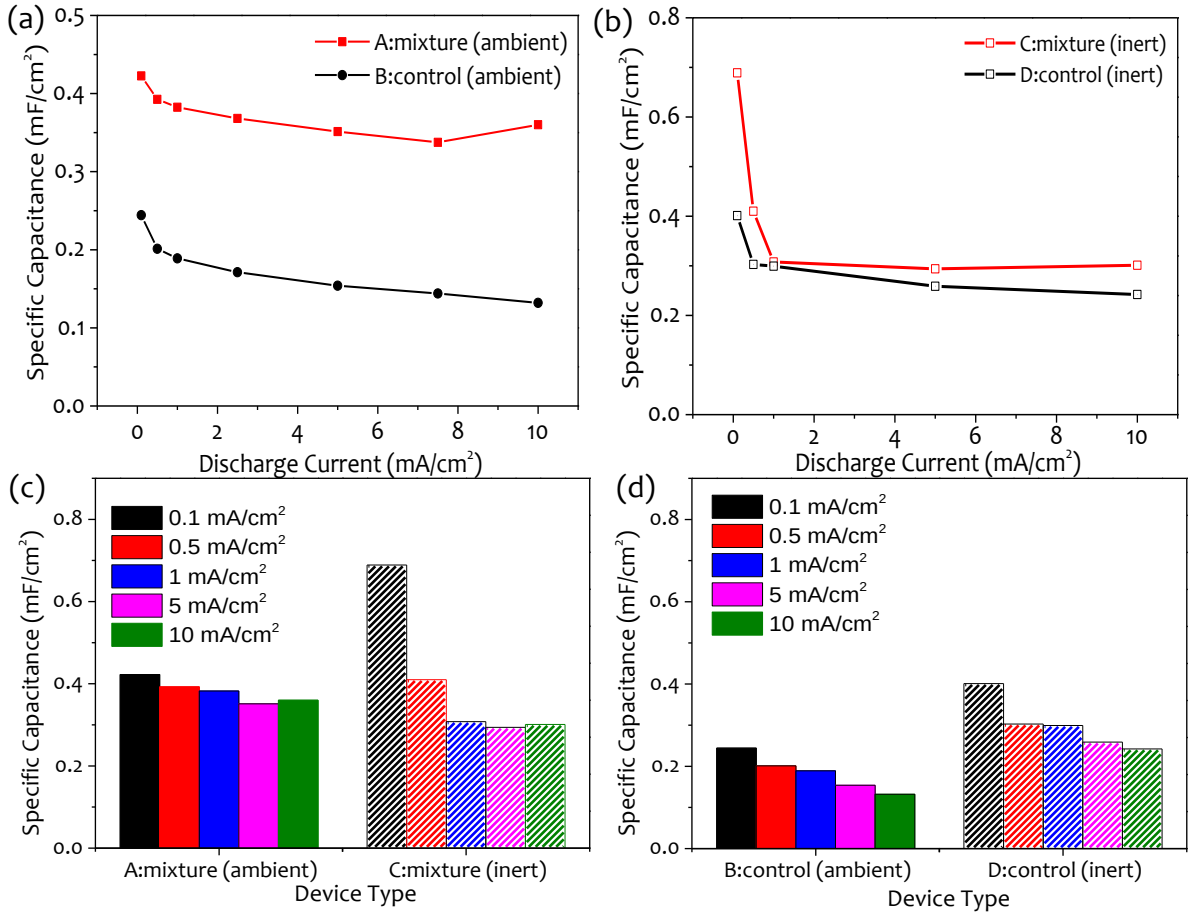

Figure 4.8: Specific capacitance at different discharge current of devices assembled in (a) ambient and (b) inert atmosphere. Bar graph representation of specific capacitance of (c) device A: mixture (ambient) and C:mixture (inert), (d) device B:control (ambient) and D:control (inert) at variable current density.

Interestingly, comparison of both devices in wet state, A and B assembled in ambient show that device A with electrolyte mixture exhibit higher discharge time and higher specific capacitance (relative increase of 102%) than device B which is lesser in inert conditions (Figure 4.8a). These results are also in conjugation with the CV measurements which show superior electrolytic behaviour of F-TEDA in $TBABF_4$ (Figure 4.4 and 4.6). As seen in Figure 4.8c, device A outperforms device C in terms of specific capacitance values at high current densities in spite of its lower voltage window. The specific capacitance at higher current density is observed to be higher for device A compared to device C despite of higher voltage of 1.8 V in case of device C as compared to A (0.8 V). On contrary, the capacitance of device D: control (inert) in comparison to that of device B: control (ambient) is higher as expected due to the wider voltage window of 1.8V (Figure 4.8d).

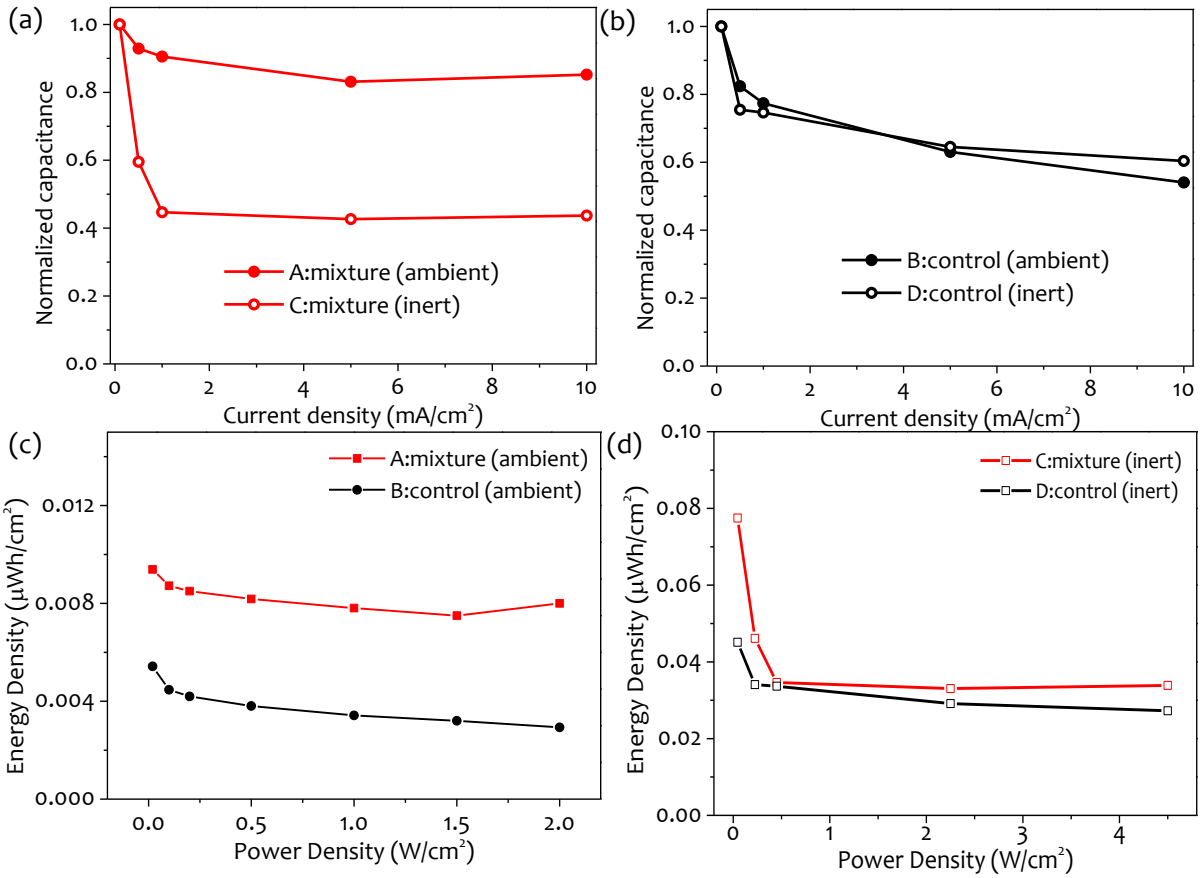

Figure 4.9: Normalized capacitance retention of (a) A:mixture (ambient) and C:mixture (inert), (b) B:control (ambient) and D:control (inert) at variable current density. Ragone plot of devices assembled in (c) ambient and in (d) inert condition.

Among all the devices, device A shows the highest capacitance retention of 85.7% over the entire range of current density from 0.1–10 mA/cm² (Figure 4.9a).The capacitance retention at high current densities is clearly an indicative of formation of stable electric double layer capacitor that retains its capacitive behaviour even at ultra-high charging and discharging rates. Moreover, there is no significant change in the capacitance retention property of devices B and device D (Figure 4.9b). Device A has higher capacitance retention in comparison to device D due to the contribution of F-TEDA electrolyte despite of the presence of water molecules in ambient conditions in A. The energy density and power density values for all the devices were calculated and Ragone plots for all the devices are shown in Figure 4.9c,d. For the devices prepared under ambient conditions, a relative increase of 172.72% in energy density at power density of 2 W/cm² was observed for device A with mixture electrolyte in comparison to control device B clearly highlighting the influence of F-TEDA on device performance (Figure 4.9c). However, for the devices fabricated inside the glove box, the relative difference in energy density values for both the electrolytes was not very significant (Figure 4.9d). For both mixture as well as control device, C and D respectively, the performance is better in the inert atmosphere due to higher voltage window of 1.8 V. The power density and energy density is proportional to square of voltage that leads to an overall high performance under inert conditions.

4.3.5 Cyclic Stability

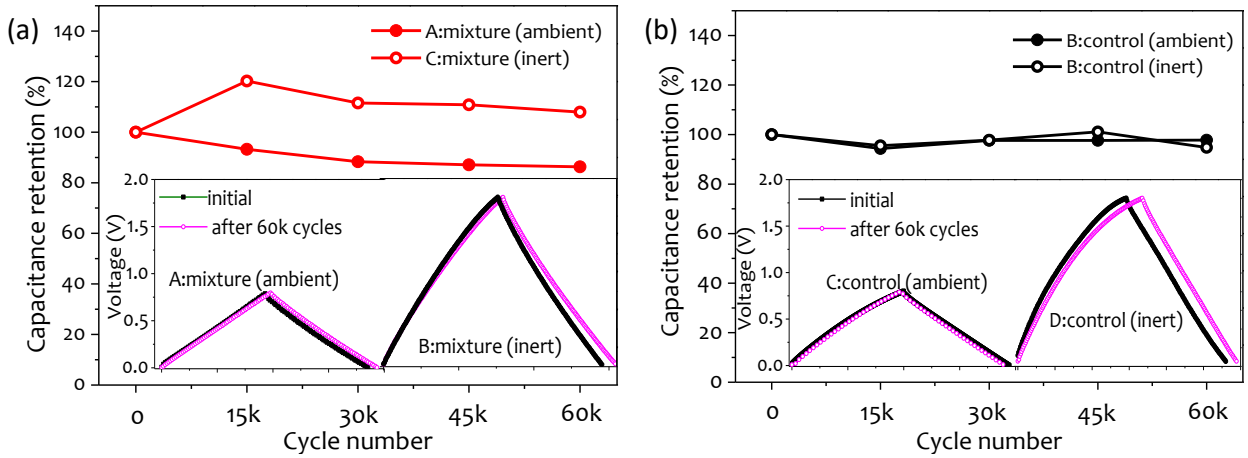

Figure 4.10: Capacitance retention over 60,000 cycles for (a) A:mixture (ambient) and C:mixture (inert), (b) B:control (ambient) and D:control (inert) at applied current density of 1 mA/cm^2 . Inset Figure 4.10 (a) and (b) show GCD curve of before and after 60,000 cycles for the corresponding device.

Long life cycling is an important factor for evaluation of the performance of the supercapacitor. Cyclability test for all the devices were performed at a current density of 1 mA/cm^2 for 60,000 cycles. The charge discharge curves for all the devices before and after 60,000 cycles are shown in insets of Figure 4.10a and b. For the devices prepared with mixed electrolyte (device A and C), the device A prepared in ambient exhibits a small but gradual decrease in specific capacitance with 86% capacitance retention at 60,000th cycle. Whereas, device C assembled under inert conditions show a jump in initial capacitance followed by a gradual decrease upon cycling. The increase in initial capacitance could be due to improved wettability of electrode by repeated cycling. In case of $TBABF_4$ based devices, both devices exhibit excellent cyclability with retention of capacitance of ~ 95% over the entire cycling range (Figure 4.10, Table 4.2). Overall, the cyclic stability of device C with mixed electrolyte in inert is superior and shows an overall increase in capacitance even after 60,000 cycles which is a remarkable aspect in this study. The differences in the capacitive behaviour of all the supercapacitors are tabulated in Table 4.2.

Table 4.2: Comparative performance of fabricated supercapacitors

Characteristics of Devices	Electrolyte Mixture		Control	
	A:mixture (ambient)	C:mixture (inert)	B:control (ambient)	D:control (inert)
Voltage Window (V)	0.8	1.8	0.8	1.8
C_{sp} at 0.1 mA/cm^2 (in mF)	0.42	0.69	0.24	0.4
Capacitance Retention (%)*	85.7	44.1	60	54.1
Capacitance Retention (%)$^{\#}$	86.3	107.9	97.8	94.8

*over 0.1 -10 mA/cm^2 (%); $^{\#}$over 60,000 cycles

Interestingly, the moisture has a very strong influence on the overall performance of F-TEDA in electrolyte mixture as reflected from the comparison of device A with devices B and C. Device A display a relative increase of 102% in specific capacitance with respect to device B.

4.3.6 Electrochemical Impedance Analysis

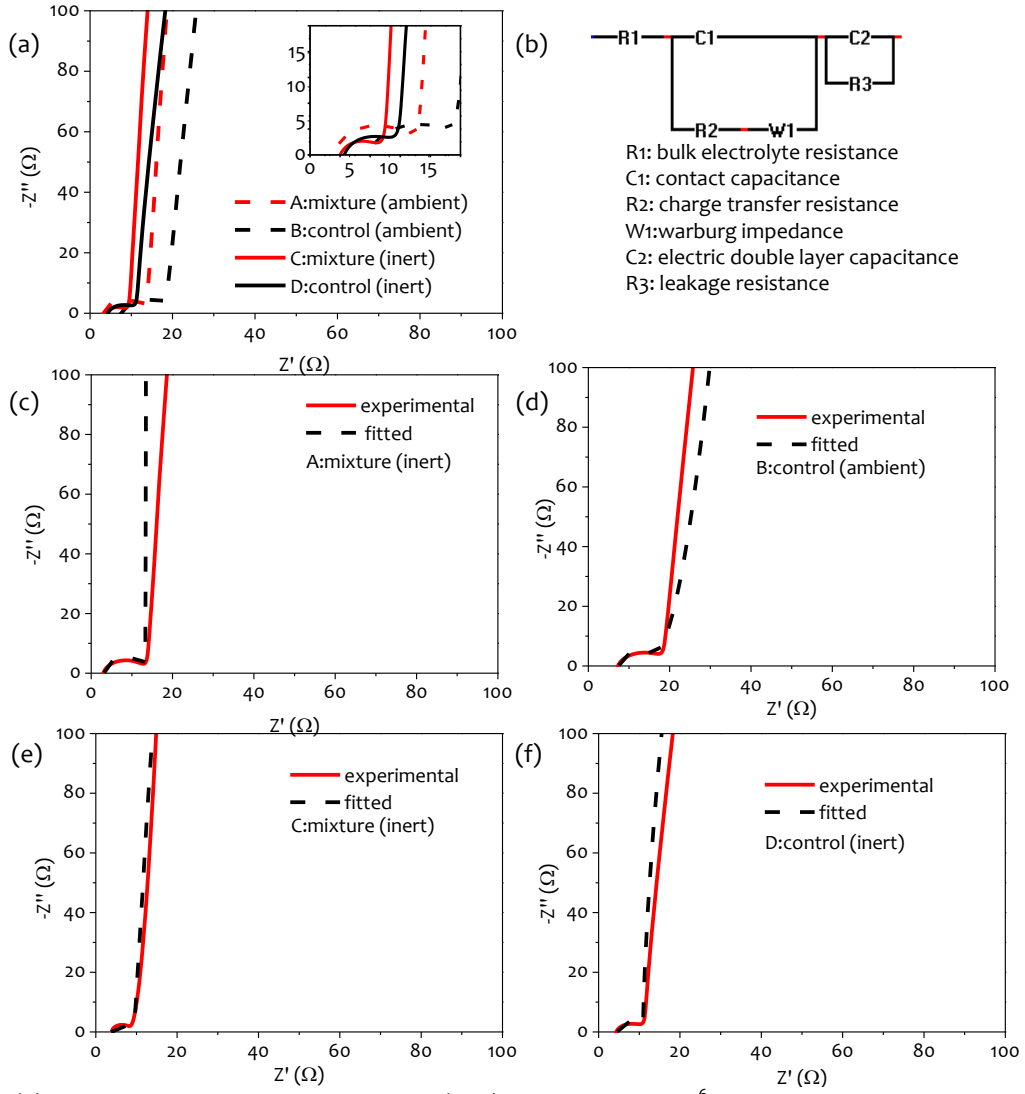

Figure 4.11: (a) Nyquist plot of fabricated devices (A-D) taken over 0.1-10^6 Hz frequency range. Inset shows the magnified Nyquist plot at higher frequency. (b) Nyquist equivalent circuit with parameters. Experimental and fitted Nyquist plots of (c) A:mixture (ambient), (d) B:control (ambient), (e) C:mixture (inert) and (f) D:control (inert).

Electrochemical impedance analysis (EIS) was performed over 0.1 Hz-10^6 Hz frequency range to understand the working of the fabricated supercapacitors. All the assembled devices show the signature capacitive Nyquist behavior of a semicircle at high frequency with a near perpendicular line at low frequency region (Figure 4.11a). The EIS data for all the devices were fitted using conventional EDLC equivalent circuit[Lei et al., 2013] (Figure 4.11b) and the resistance values analyzed (Figure 4.11c-f). For the assembled devices, A:mixture (ambient) shows lowest electrolytic resistance, R_S (3.1 Ω) which is evident from the intercept of corresponding semicircle in the Nyquist plot. $TBABF_4$ based device B in ambient condition shows much higher electrolytic resistance (R_S= 7.5 Ω) signifying the superior electrolytic behaviour of F-TEDA mixed electrolyte in ambient conditions. The difference in electrolytic resistance for the devices C and D assembled under inert atmosphere is small (4.0 Ω and 4.6 Ω respectively) indicating poor mobility of F-TEDA in absence of moisture.

Further, electrochemical impedance analysis can also be used to understand the kinetics of the electrolyte ion diffusion process occurring across the electrode interface. The diameter of the semicircle in the Nyquist plot shown in inset Figure 4.11a is used to derive the resistance across the electrolyte-electrode interfaces.[Lei et al., 2013] The devices A and B assembled in ambient shows much higher electrode-electrolyte resistance, R_{CT} (10.1 Ω and 8.2 Ω respectively) in

comparison to devices C and D assembled in inert (R_{CT} of 4.3 Ω and 4.6 Ω respectively). The high electrolyte-electrode interface resistance of devices A and B is probably due to the water solvation sphere around the ions thus retarding the diffusion of ion across the interface. Since device A exhibits higher R_{CT} than device C, the device C exhibits better rate capability than device A even though it has lower Rs. These observations clearly indicate the superior capacitive behaviour of F-TEDA containing electrolyte under inert conditions.

4.3.7 Electrolyte Performance with Graphene Petal Electrodes

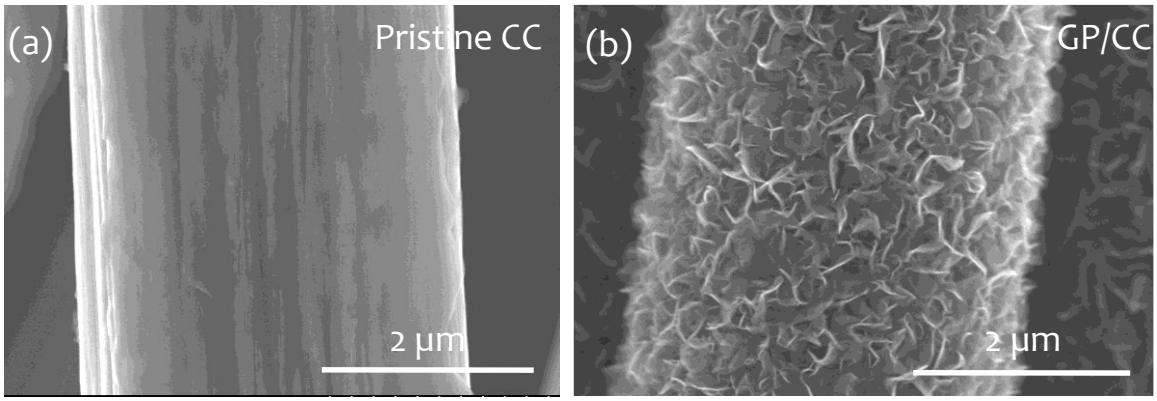

Figure 4.12 SEM image of pristine (a) carbon cloth (CC) and (b) graphene petals on carbon cloth (GP/CC)

Vertically oriented 3D graphitic nanopetals (GP) on carbon cloth was also explored as 3D electrode system for the electrolyte developed in this study. [Gupta et al., 2016a; Xiong et al., 2014, 2016]. The growth of vertically oriented 3D graphene on carbon cloth was analyzed by the Scanning Electron Microscopy (SEM). Highly uniform, high surface area and vertically oriented 3D graphene petals grown on carbon cloth can be seen in Figure 4.12.

For analyzing the electrolyte performance in high surface area electrodes, supercapacitor devices were fabricated in inert and ambient conditions using graphene petals on carbon cloth as the electrode material. It was very interesting to observe that the devices show similar behavior of sensitivity towards water for mixture electrolyte. The CV plots in Figure 4.13 a, b, d, e show a significant increase in current for mixture electrolyte in ambient conditions than that observed in the devices fabricated in inert conditions.

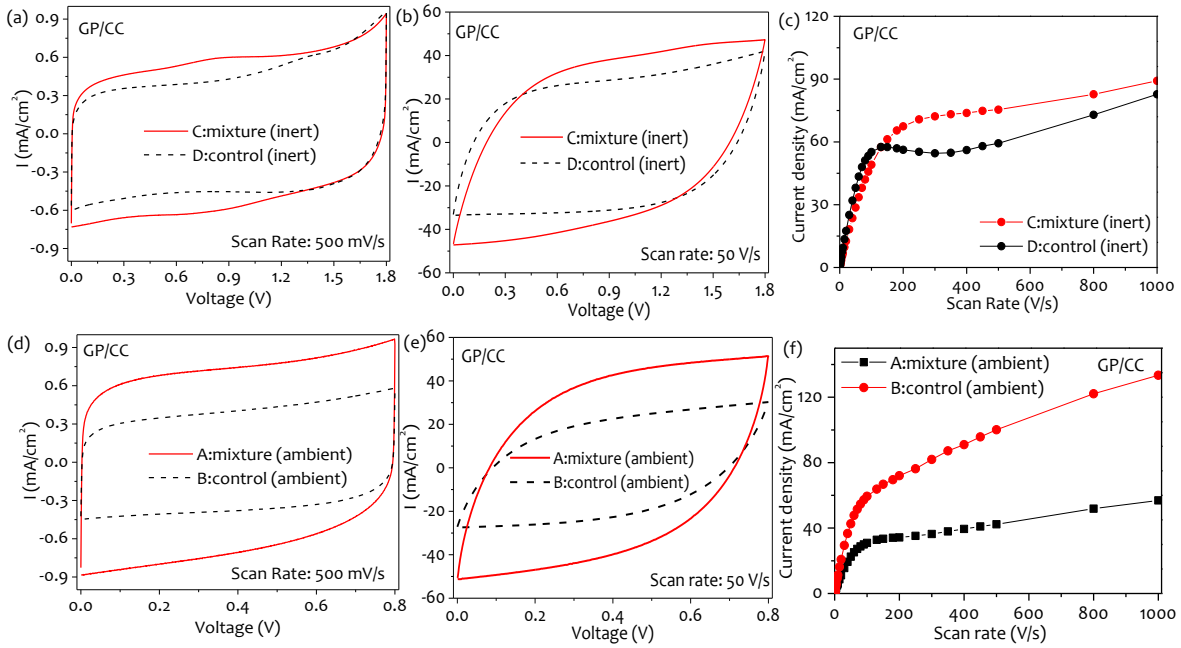

Figure 4.13 Comparative cyclic voltammetry curves of supercapacitors assembled with graphene petals on carbon cloth (GP/CC) in (a,b) inert and (d,e) ambient condition at scan rates of 0.50 V/s, 50 V/s respectively. Current density at 0.9 and 0.4 V for varying scan rates of 0.02-1000 V/s in (c) inert and (f) ambient conditions.

Additionally, due to higher surface area, the devices show ~1 order higher specific capacitance in comparison to pristine carbon cloth electrodes. For GP/CC as electrode material, with the increase in the scan rate, a non-linear response after 150 V/s is observed which could be understood due to the porous electrode material which dominates the electrolytic behaviour at ultrahigh scan rates. (>150 V/s) (Figure 4.13 c and f).

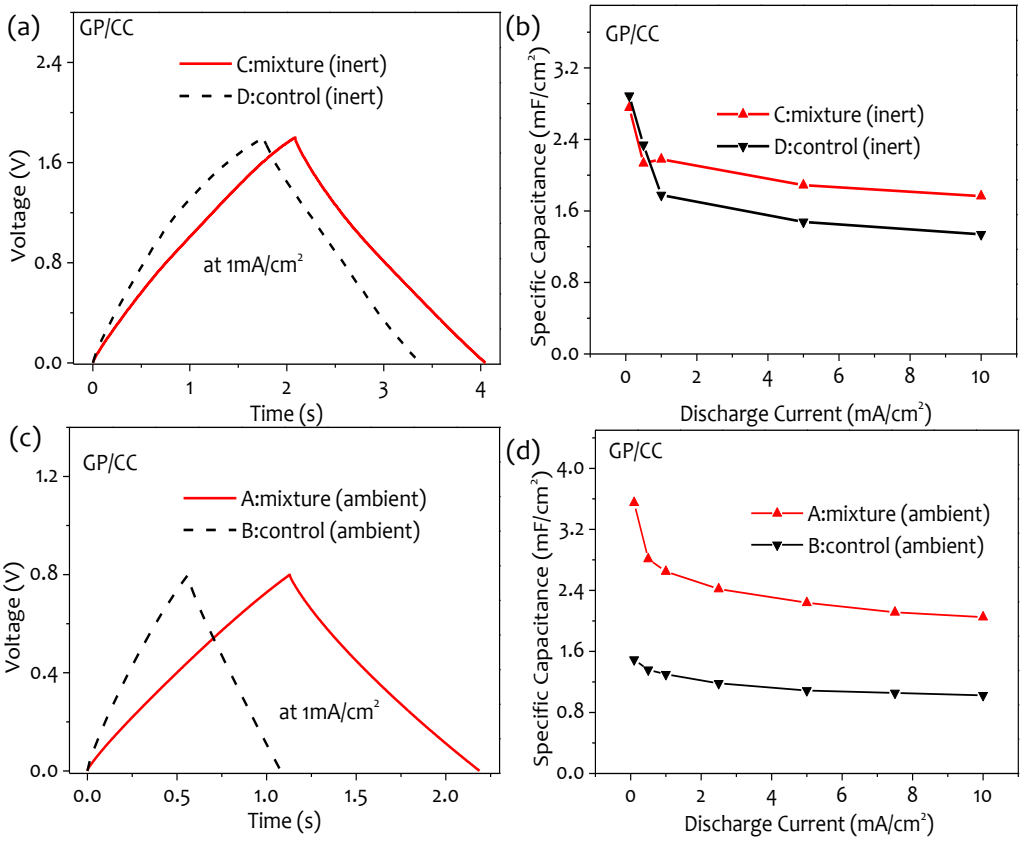

Figure 4.14 Galvanostatic charge/discharge (GCD) curves of supercapacitors with GP/CC electrodes at current density of 1 mA/cm² in (a) inert (c) ambient conditions. Specific capacitance at different discharge current of devices assembled in (b) inert and (d) ambient atmosphere.

GCD measurements were also performed on the devices prepared with GP/CC as electrode material to analyze the charging and discharging behavior. As expected the devices show symmetrical GCD response with negligible IR drop pointing towards the potential synergy of the mixture electrolyte with high surface area electrolyte material (Figure 4.14 a and c). Furthermore, in ambient the mixture electrolyte shows much higher capacitance increase in comparison to that of control. It is very interesting to notice that the device with mixture electrolyte prepared at ambient show higher capacitance that that prepared in inert in-spite of the reduced voltage window (Figure 4.14 b and d). Hence, a new electrolyte system has been explored for both low and high surface area electrodes with enhanced performance in comparison to that of conventional electrolyte that can be operated at a wide charging discharging rate. Further, the device performance is influenced by the moisture content present in the atmosphere.

4.4 Conclusions

In conclusion, an organo-fluorine compound is explored as a novel electrolyte system for construction of electric double layer supercapacitors. The limited solubility of F-TEDA/$TBABF_4$ mixed electrolyte in acetonitrile resulted in an electrolyte with low concentration of ~0.5 M however the capacitance not only depends on the number of ions but also the mobility of ions in between the electrodes. The device fabricated with F-TEDA based electrolyte displayed higher

capacitance and ultrafast rate capability with low time constant. The device performance was better under inert conditions in terms of increase in voltage window to 1.8 V and higher cyclic stability tested over 60,000 cycles. Under ambient condition, when the electrolyte is in wet state, device with mixture electrolyte shows a relative increase by 102% and 172.7% in specific capacitance and energy density in comparison to $TBABF_4$ as control, however the voltage window was restricted to 0.8 V thus limiting the overall energy and power density. This study explores the strength of F-TEDA as an electrolyte in supercapacitors and further opens up scope for new fluorine containing electrolytes in energy storage devices for enhanced performance. Clearly, the advantage of using F-TEDA as an additive is reflected in the improved performance in terms of specific capacitance and rate capability. Similar additives containing N-F bond with higher solubility could be explored to further enhance the performance. The operating window can be extended by using ionic liquids as support electrolyte.